

Depth-to-the-bottom optimization for magnetic data inversion: Magnetic structure of the Latium volcanic region, Italy

F. Caratori Tontini,¹ L. Cocchi,² and C. Carmisciano¹

Received 13 October 2005; revised 14 June 2006; accepted 17 July 2006; published 17 November 2006.

[1] We present an algorithm for the linear inversion of two-dimensional (2-D) surface magnetic data to obtain 3-D models of the susceptibility of the source. The forward model is discretized by a mesh of prismatic cells with constant magnetization that allows the recovery of a complete 3-D generating source. As the number of cells are normally greater than the amount of available data, we have to solve an underdetermined linear inverse problem. A Tikhonov regularization of the solution is introduced as a depth-weighting function adapted from Li and Oldenburg (1996) to close the source toward the bottom. The main novelty of this method is a first-stage optimization that gives information about the depth to the bottom of the generating source. This parameter permits both the evaluation of the appropriate vertical extension of the mesh and the definition of the shape of the regularizing depth-weighting distribution. After discussing the performance of this method by showing the results of various synthetic tests, we invert the magnetic anomalies of the volcanic edifices in the Latium region in central Italy to define their 3-D source distribution.

Citation: Caratori Tontini, F., L. Cocchi, and C. Carmisciano (2006), Depth-to-the-bottom optimization for magnetic data inversion: Magnetic structure of the Latium volcanic region, Italy, *J. Geophys. Res.*, *111*, B11104, doi:10.1029/2005JB004109.

1. Introduction

[2] The quantitative estimation of the physical parameters of the source generating an observed potential-field anomaly is an inverse problem. Functionals relating a particular distribution of magnetic susceptibility to the observed anomaly are usually not analytically invertible, and furthermore, even after linearization, the number of unknowns often exceeds the number of observations. Inverse problems of this kind are characterized by instability and nonuniqueness of the solution [Tikhonov and Arsenin, 1977; Tarantola, 1987; Menke, 1989]. The theoretical or inherent ambiguity has been known since Gauss' epoch as a trivial consequence of the Laplace equation [Blakely, 1995]. Algebraic ambiguity is another major concern. We follow the frequently used procedure that consists of subdividing the region presumably containing the source into a set of prismatic volume pixels (voxels). The relationship connecting the magnetization of each voxel with the observed datum is thus linear and can be represented by a sensitivity matrix. This matrix is always rank deficient: thus it has a multidimensional null-space. The solution of this problem is an affine space of vectors, in the sense that a particular solution can be perturbed by a vector that spans the null-

space of the matrix (also called its annihilator) without changing the resulting anomaly. Experimental ambiguity finally, comes from geological or experimental noise in the data that always affects the resolution of the model and may generate spurious sources. All of the above considerations apply to inversions for density perturbations from gravity anomalies as well as to inversions for magnetic susceptibility from magnetometer observations, on which we focus mainly in this paper.

[3] We recall that the forward model may be unable to represent the source exactly. In the case of a spherical source meshed by prismatic voxels the problem is one of incompatibility of the system of equations rather than ambiguity. As a consequence of these ambiguities and incompatibilities "optimal solutions" may arise at any depth, which accounts for the widely perceived notion that potential-field data lack depth resolution and that the inverse modeling often yields solutions that are too shallow. To obtain realistic models additional information has to be introduced, known as "a priori" information, in the statistical (Bayesian) sense, or as regularization in the sense defined by Tikhonov and Arsenin [1977]. These approaches have been interpreted as different alternatives [Scales and Snieder, 1997], but they may in fact be compatible under certain restrictive assumptions [Ho-Liu *et al.*, 1989; Yanovskaya and Ditmar, 1990; Simons *et al.*, 2002].

[4] Several approaches that deal with the problems of nonuniqueness of potential-field inversion exist [Boulanger and Chouteau, 2001; Silva *et al.*, 2001]. Minimization of the total volume [Last and Kubik, 1983] or of the moment

¹Stazione di Geofisica Marina, Istituto Nazionale di Geofisica e Vulcanologia, Fezzano, Italy.

²Dipartimento Scienze della Terra Geologiche-Ambientali, Università di Bologna, Bologna, Italy.

of inertia [Guillen and Menichetti, 1984] of the source allows the recovery of compact models by avoiding dispersion of the source. Barbosa and Silva [1994] obtained compactness along several axes by introducing “a priori” information about the axis length. Caratori Tontini et al. [2003] developed a model based on the envelope of the source by using a set of three-dimensional (3-D) Gaussian functions. Fedi and Rapolla [1999] studied a multilayer 3-D data set, obtaining solutions at the correct depth by studying also the vertical variations of the magnetic field. In this vein we also note the work of Jacobsen [1987] and Pedersen [1991], who concluded that “the difference of the fields upward continued to different levels represents the best estimate of the field from the depth interval which is half of the upward continued height interval”.

[5] In their very interesting paper, Li and Oldenburg [1996] introduced a depth-weighting function to counteract the spatial decay of the kernel function with depth, giving increasing weight to voxels at increasing depths. Together with global smoothness constraints these authors obtained compact solutions and reduced the dispersion of the source along the three spatial directions, recovering thus a model with a “minimum structure”. Depth-weighting has given meaningful results and has been applied successfully into other inversion algorithms [Pilkington, 1997; Boulanger and Chouteau, 2001; Portniaguine and Zhdanov, 2002; Zhdanov, 2002; Pignatelli et al., 2006], since it allows the user to obtain solutions at the correct depths even in the case of vertically dislocated sources.

[6] Our work is built on the study of Li and Oldenburg [1996]. The guidelines we adopted were mainly dictated by the requirement of a straightforward and easy-to-use algorithm, with good performance in terms of execution times and robustness in the presence of noise. This is particularly useful for direct real-time applications during the survey execution, where we have few information about the source and the data quality is not fully enhanced. The easiness of implementation is particularly suitable for anyone interested to reproduce or to increase the capability of the method. To this aim we introduce a depth weighting of the model norm without additional constraints in order to reduce to a minimum level the amount of required “a priori” information. This allows the user to get fast first-order approximation solutions which can show, however, important information about the susceptibility distribution, the structural trends of the source and the depth distribution, especially concerning the bottom characterization. This choice allows the transformation of the problem into a “free” inversion with a new sensitivity matrix, increasing the numerical performance of the method.

[7] We will show that the inverse models are pushed toward the bottom of the mesh, even if the relative depths between sources are preserved. Depth-weighting alone is thus unable to give a solution with a correct depth to the bottom (DTB) of the source, and additional information should be added. As far as we know, the exact introduction of the DTB parameter in the framework of 3-D linear inversion has not been directly treated by previous methods, while often the depth to the top is properly found when using a standard depth-weighting distribution. Resolving the DTB, however, is important not only because it may define the magnetic basement, but also because it permits

the definition of an appropriate mesh for the inversion with minimum vertical extent. We thus modify the depth-shape distribution in the regularization matrix by combining a depth-weighting function, based on a power law decay, with a function that allows the closure of the solutions at a consistent bottom depth. In other words, our method finds a regularization matrix that depends on one parameter related to the DTB of the source.

[8] Moreover enough information is contained in the data itself to find this parameter by the preliminary minimization of a new norm of the solution, which we introduce in this paper. In practice we have adopted a regularization which uses the minimum amount of “a priori” information needed for an essential characterization of the source, especially in terms of depth-shape and susceptibility distribution, letting the algorithm being sufficiently fast and easy to use, but also flexible, to be upgraded by additional constraints or optimization improvements if needed by the user. This demonstrates also that when the Tikhonov regularization is adapted with a meaningful depth function, potential-field data can provide DTB information without imposing additional constraints or requiring more “a priori” information. We show the above on the basis of synthetic tests and also by inverting the magnetic anomalies of the volcanic centers of Latium in central Italy.

2. Inverse Model

[9] We group the observations into a column vector \mathbf{d} , while the parameters that are the target of the inversion are identified by the vector \mathbf{p} that consists of the magnetic susceptibility of each voxel, within a 3-D mesh grid presumably containing the true source. The elements of the vector \mathbf{p} are ordered in function of increasing depth, in the direction of the layers of the mesh. The linear forward model is expressed in the following equation

$$\mathbf{d} = \mathbf{K} \cdot \mathbf{p}, \quad (1)$$

where \mathbf{K} is the sensitivity matrix that expresses the contribution of a single voxel of the mesh to a particular observed datum. The column index j of \mathbf{K}_{ij} indicates the contribution of the j th prismatic voxel of the mesh to the i th observation, i.e., the magnetic field generated in the spatial position of the i th observation by the j th prismatic voxel, as if the voxel was uniformly magnetized. This matrix is evaluated according to Bhattacharyya [1964], who derived analytical relationships for the magnetic field generated by a rectangular prism. The magnetic theory being linear, the field at the spatial position of the i th observation is given by the sum of all the contributions of each j th voxel weighted with its specific susceptibility p_j , as in equation (1). As we will see, we look for two main sets of parameters: a preliminary optimization step gives the DTB of the source, while the final result is the 3-D spatial distribution of the susceptibility \mathbf{p} .

[10] We introduce further the hypothesis of induced magnetization, namely that the ambient geomagnetic field has the same direction as the source magnetization. This is a well-justified hypothesis since many anomalies are generated by sources whose magnetization is induced by the ambient field itself. Otherwise an average remanent mag-

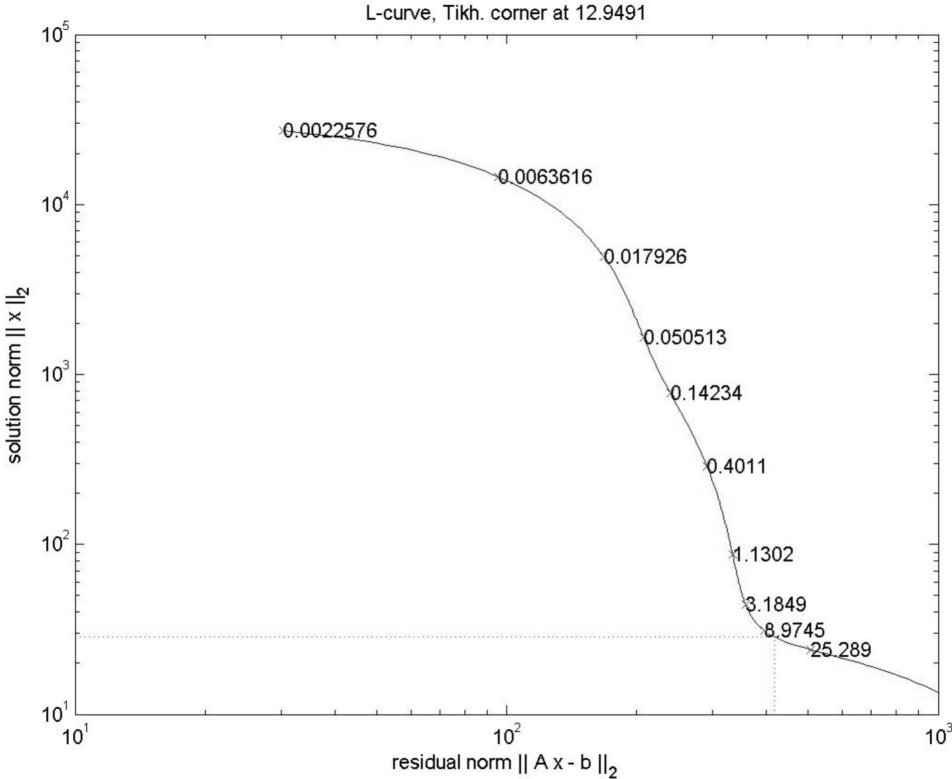


Figure 1. L curve obtained inverting the synthetic anomaly of Figure 2. Along the curve are drawn the λ values. The corner of the curve, that is, the maximum curvature point, corresponds to the optimal $\lambda = 12.9491$. This value, as can be seen in this qualitative figure, represents a good compromise between data fitting and small norm of the solution. The chi-square norm is 420. Having inverted 400 data, we obtained a reduced chi-square norm 1.05 that corresponds to a significance level of 75%.

netization direction has to be properly evaluated and introduced in the sensitivity matrix [Helbig, 1963; Claerbout, 1976; Andersen and Pedersen, 1979].

[11] The linear operator \mathbf{K} has a multidimensional null-space. The solution thus has to be regularized [Tikhonov and Arsenin, 1977]. To this aim we adopt the very useful set of Matlab routines developed by Hansen [1994]. The optimal solution \mathbf{p}_{opt} minimizes the misfit between the observed data and the anomaly generated by the recovered model in a chi-square sense, with the additional constraint of minimizing also a particular regularizing norm:

$$\mathbf{p}_{opt} = \arg \left(\min \left\{ |\mathbf{K} \cdot \mathbf{p} - \mathbf{d}|^2 + \lambda^2 |\mathbf{L} \cdot \mathbf{p}|^2 \right\} \right), \quad (2)$$

where \mathbf{L} is a square matrix, whose dimension equals the number of unknown parameters. The Lagrange multiplier λ should represent a compromise between data fitting and norm of the solution. Large values of λ generate very compact solutions at the expense of a large chi-square norm that indicates poor data fit; instead lower values of λ generate solutions that, while fitting very well the data, in many cases are far from the true model. We choose the optimal λ value according to the L curve principle [Lawson and Hanson, 1974; Hansen and O'Leary, 1993]. The L curve is a plot of $\log |\mathbf{L} \cdot \mathbf{p}|^2$ versus $\log |\mathbf{K} \cdot \mathbf{p} - \mathbf{d}|^2$. This curve is L shaped, with the optimal λ in a distinct corner, that is, the point of maximum curvature.

[12] An example of this particular behavior can be seen in Figure 1, where we show the L curve that corresponds to the inversion of the synthetic anomaly of Figure 2. We announce in advance that this inversion was performed by using $n = 400$ data. In proximity of the optimal $\lambda = 12.9491$ the chi-square norm χ^2 is 420, and thus the reduced chi-square norm (χ^2/n) is 1.05, indicating a good fit. Quantitatively speaking this result translates into a significance level of 75%, i.e., the probability that a value of χ^2 at least as large as 420 will be obtained within a large number of experiments. These results allow thus the interpretation of the optimal λ value as a good balance between data fitting and norm of the solution.

[13] A common practice in inverse problems is to identify \mathbf{L} with the identity matrix. This corresponds to finding the minimum L^2 norm solution of the linear problem. Li and Oldenburg [1996] showed that in potential-field inversion this is unsatisfactory since the solution tends to be clustered toward the top of the mesh, where low values of density or magnetization can fit the observed data very well. We design a regularization matrix \mathbf{L} that generates solutions at a consistent depth. Li and Oldenburg [1996] corrected the radial decay of the kernel by using an empirical function that simulates the decay of the magnetic field with depth. Following them, we assume a diagonal form for \mathbf{L} , such that

$$\mathbf{L}(z)_{ij} \equiv F_{reg}(z) \delta_{ij}, \quad (3)$$

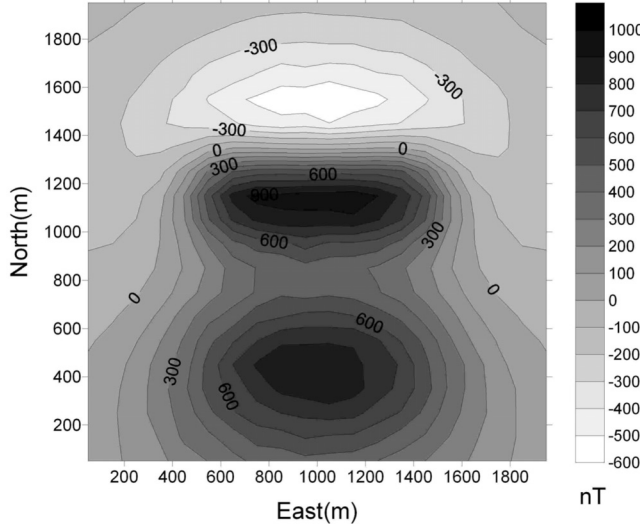


Figure 2. Synthetic anomaly generated by a composite prismatic model. The inducing field is assumed having an inclination of 60° , a declination of 0° , and a magnitude of 46,000 nT. The anomaly is calculated by a grid of 20×20 points. Random Gaussian noise with a standard deviation of 3% of the data amplitude has been added to the data.

where δ_{ij} is the Kronecker symbol and $F_{reg}(z)$ indicates the function expressing the contribution of a horizontal layer of the mesh at the depth z , normalized to its maximum over all depths. The first-order approximation of the function $F_{reg}(z)$ is

$$F_{reg}(z) \approx \frac{l_z^{3/2}}{z^{3/2}}, \quad (4)$$

where l_z is the vertical extension of the mesh, and the depth z is measured from the top of the mesh to the center of the

layer to avoid singularities in equation (4). As shown by Li and Oldenburg [1996] the choice of the depth function is empirical. In particular, the use of a greater exponent in equation (4) flattens the solution too much toward the bottom of the mesh, without preserving the vertical ratios between depths of separate sources. Lower values of the same exponent instead produce too shallow results. By using equations (3) and (4) we next define

$$\mathbf{p} \equiv \mathbf{L}^{-1}(z) \cdot \mathbf{p}', \quad (5)$$

which emphasizes the deep layers of the mesh given the increasing values of $\mathbf{L}^{-1}(z)$ with depth. Being diagonal and having nonzero values on the diagonal $\mathbf{L}(z)$ is invertible, and equation (2) takes on the following form

$$\mathbf{p}'_{opt} = \arg \left(\min \left(\{ |\mathbf{K} \cdot \mathbf{L}^{-1} \cdot \mathbf{p}' - \mathbf{d}|^2 + \lambda^2 |\mathbf{p}'|^2 \} \right) \right). \quad (6)$$

Practically the solution of equation (6) is obtained by a simple SVD decomposition that gives the minimum L^2 norm solution of a problem with a new sensitivity matrix $\mathbf{K} \cdot \mathbf{L}^{-1}$. The correctness of equation (6) is simply established by the following steps

$$\begin{aligned} \min \left\{ |\mathbf{K} \cdot \mathbf{L}^{-1} \cdot \mathbf{p}' - \mathbf{d}|^2 + \lambda^2 |\mathbf{p}'|^2 \right\} &= \\ \min \left\{ |\mathbf{K} \cdot \mathbf{L}^{-1} \cdot \mathbf{p}' - \mathbf{d}|^2 + \lambda^2 |\mathbf{L} \cdot \mathbf{L}^{-1} \cdot \mathbf{p}'|^2 \right\} &= \\ \min \left\{ |\mathbf{K} \cdot \mathbf{p} - \mathbf{d}|^2 + \lambda^2 |\mathbf{L} \cdot \mathbf{p}|^2 \right\}, \end{aligned} \quad (7)$$

where having used equation (5) together with the identity matrix in the form of $\mathbf{L}^{-1} \cdot \mathbf{L}$, we show that the process is equivalent to finding a solution that gives emphasis to greater depths as in equation (2). Equation (7) agrees with the results of Boulanger and Chouteau [2001] and

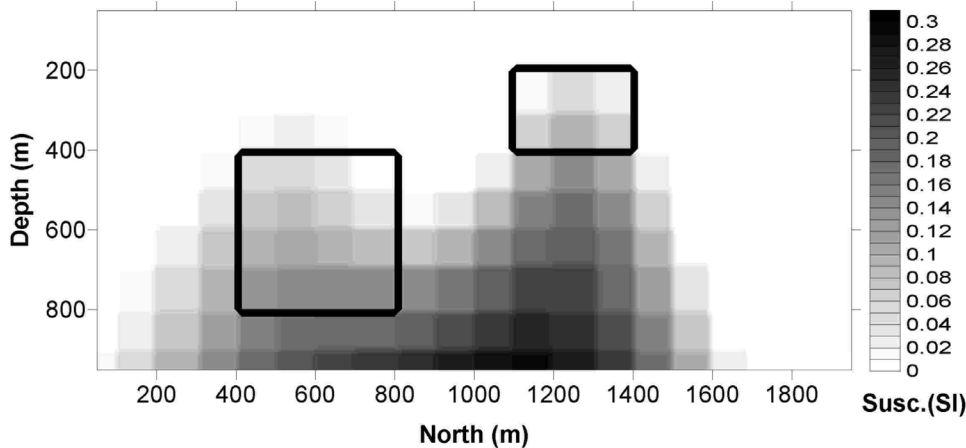


Figure 3. Central section showing the result of the inversion of the anomaly of Figure 1 by using a power law decay regularization matrix. The true source is represented by the thick boxes and has a susceptibility of 0.3 (SI). The recovered model is far from the true model, since it tends to flatten the solution toward the bottom of the mesh. Nevertheless, it seems to resemble the depth ratios of the true model, in the sense that a shallower source is found where the upper prism is located.

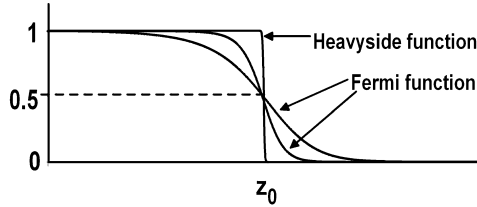


Figure 4. Comparison between the Heaviside step function and its approximated differentiable version given by the Fermi function. Greater values of Δz generate greater thicknesses around which the function annihilates itself.

Pignatelli et al. [2006], where the sensitivity matrix has been directly corrected by multiplying it with a power law function that increases with depth. We find the minimum L^2 norm solution \mathbf{p}'_{opt} , and finally the correct vector $\mathbf{p}_{opt} \equiv \mathbf{L}^{-1}(z) \cdot \mathbf{p}'_{opt}$.

[14] As it turns out, this regularization is insufficient, even if in the case of vertically dislocated sources it preserves the difference in depth. In Figure 2 we show the magnetic anomaly generated by a source made of two prismatic bodies buried at different depths, while Figure 3 shows a vertical northward oriented cross section with the result of the inversion compared with the true sources. We have inverted 20×20 data contaminated by random Gaussian noise with a standard deviation of 3% of the data amplitude by using a mesh of $20 \times 20 \times 10$ voxels centered under the anomaly. We show only the relevant central cross section since the source is characterized by a strike length along the y axis of 1000 m. The recovered solution is far from the true model because the chosen regularization tends to put the maxima of the magnetization toward the bottom of the mesh. However, the shape of the solution has a certain resemblance to the ratios of depths between the real sources.

[15] Our solution is now to introduce a correction term in the regularization that allows the exact evaluation of the depth to the bottom of the solution. We correct thus the regularization matrix by closing it toward the bottom of the mesh according to the following equation:

$$\mathbf{L}^{-1}(z)_{ij} \equiv F_{reg}^{-1}(z) \cdot B(z) \cdot \delta_{ij}, \quad (8)$$

where the function $B(z)$ should contain the DTB information. This function B too, is empirical, and we introduce it by practical considerations.

3. Fermi Function

[16] The choice of $B(z)$ is dictated by the requirement that it preserves the power law decay of the regularization matrix at depths shallower than the DTB of the generating source. This property is really essential to obtain the correct depth-to-the-top ratios. Below the DTB of the generating source we should obtain instead a negligible solution. The function $B(z)$ should thus have a constant unitary value at shallow depths and should annihilate itself at depths greater than the DTB of the generating

source. A good candidate is identified by the Heaviside step function (Figure 4):

$$\theta(z - z_0) = \frac{1}{2} - \frac{1}{2} \operatorname{sign}(z - z_0), \quad (9)$$

where the function $\operatorname{sign}(z - z_0)$ is 1 when $z \geq z_0$ and -1 when $z < z_0$. The nondifferentiable behavior of this function, however, makes its use difficult in the inversion. A smooth, differentiable approximation of this function is given by the Fermi function [Landau and Lifshits, 1977] plotted in Figure 4:

$$B(z) = \frac{1}{\exp\left[(z^2 - z_0^2)/(\Delta z)^2\right] + 1}. \quad (10)$$

The parameter z_0 represents the coordinate where the function is reduced to half of its maximum value, with a characteristic thickness given by Δz . Note that in the limit $\Delta z \rightarrow 0$ the Fermi function becomes the Heaviside function, and z_0 is the real DTB of the generating source. The parameter z_0 of the Fermi function is thus connected with the depth to the bottom of the source and for this reason we label it as DTB when it takes on its true value. We assume also that the thickness $\Delta z = z_0/2$, to reduce the number of parameters. This choice is a good compromise between the step behavior of the Fermi function and its smoothness and differentia-

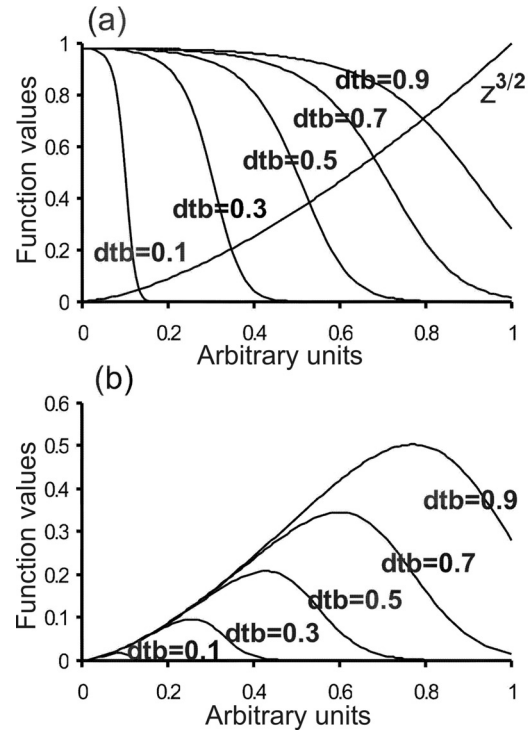


Figure 5. Plot of the regularization function for DTB values from 0.1 to 0.9 for an ideal unitary mesh. (a) Fermi functions for different values of DTB compared with the power law decay of the magnetic field. (b) Superposition of the power law decay corrected with the Fermi function. The units on the horizontal axis are arbitrary.

bility. The final version of the inverse regularization matrix is thus

$$\mathbf{L}^{-1}(z)_{ij} \equiv \frac{z^{3/2}}{l_z^{3/2} \left(\exp \left[(z^2 - z_0^2)/(z_0/2)^2 \right] + 1 \right)} \cdot \delta_{ij}. \quad (11)$$

This choice can be understood also in terms of a statistical approach of the Bayesian kind [Tarantola and Valette, 1982]. As shown by Yanovskaya and Ditmar [1990] and Simons *et al.* [2002] there is a connection between numerical regularization, for example by the Tikhonov method, and statistical addition of “a priori” information. In the Bayesian approach in particular, the vector of model parameters \mathbf{p} is distributed according to a Gaussian probability density function

$$\rho(\mathbf{p}) \propto \exp \left(-\frac{1}{2} \mathbf{p}' \cdot \mathbf{C}_p^{-1} \cdot \mathbf{p} \right), \quad (12)$$

where \mathbf{C}_p is the “a priori” model covariance matrix. As shown by Simons *et al.* [2002], the choice of a particular regularization matrix \mathbf{L} induces the same choice for the model covariance matrix

$$\mathbf{C}_p^{-1} = \mathbf{L}. \quad (13)$$

By analyzing the behavior with depth z of the regularization matrix $\mathbf{L}(z)$, expressed in equation (11), we can conclude that the “a priori” probability distribution function $\rho(\mathbf{p})$ is drastically suppressed outside of the depth range defined by the Fermi function, i.e., for depths greater than z_0 . This allows the activation of layers shallower than z_0 during the inversion.

[17] Figure 5 shows the shape of the Fermi function at various values of DTB, together with the effects of the decay factor of equation (4), evaluated on a unitary mesh. Figure 6 shows the matrix \mathbf{L}^{-1} with these characteristics for particular values of DTB. Each block represents the contribution of \mathbf{L}^{-1} for a layer of the mesh, organized at increasing depths, as the vector \mathbf{p} . The choice of a regularization matrix of this kind introduces some important characteristics within the inverted model. Particularly it describes a compact body along the vertical dimension, with a bottom depth given by the chosen DTB value. This choice generates some specific physical features in the solution, thereby reducing the ambiguity domain toward obtaining a model which is characterized by a thickness sufficient to close the source toward its bottom at a depth given by DTB. Actually the DTB value, if it is introduced by the user, represents a strong “a priori” information, which may generate realistic solutions.

[18] In the following section we will demonstrate that the parameter DTB can be estimated in a stable way from the data. The data itself thus can provide information about the depth to the bottom of the source. We will test and apply the inversion algorithm also on a case with sources at different depths and horizontal locations.

4. Determining the Regularization Parameter DTB: Synthetic Tests

[19] The choice of different values of DTB allows the closure of the solution at different bottom depths: larger

values of z_0 generate deeper sources. In Figure 7 we have inverted the field generated by a synthetic source described by a prism at a given depth in the range $z \in [300; 700]$ m. Different inversions have been performed by using different values of the DTB parameters. The mesh was made of $20 \times 20 \times 10$ cubic voxels centered about the anomaly, with a cell size of 100 m. The data have been again contaminated by random Gaussian noise. As we can see from Figure 7 we obtain solutions that are placed at different depths according to the values of DTB. The optimal value of DTB, represented by the plots where maximal magnetization values are placed inside the synthetic prism, is ideally located around 700 m, in good agreement with the depth to the bottom of the true source. It is interesting to highlight that the reduced chi-square norm χ^2/n (not to be confused with the magnetic susceptibility χ that goes by the same symbol) for Figures 7a–7f was always close to 1, indicating a good fit independently from the chosen DTB value, while obviously the L^2 norm increases as DTB increases, since more layers are activated by the inversion algorithm.

[20] At this level, however, we still need a method to determine the DTB parameter z_0 of equation (11) from the anomaly data set. The DTB represents the bottom of the source, which provides meaningful information in many geological settings, as in the definition of the magnetic basement or the Curie temperature. Estimation of this parameter is commonly done by analyzing the long-wavelength field of the magnetic anomaly in the Fourier domain [Bhattacharyya and Leu, 1975; Shuey *et al.*, 1977; Connard *et al.*, 1983; Blakely, 1988; Okubo and Matsunaga, 1994; Maus *et al.*, 1997]. The DTB parameter is also important in the definition of the optimal dimension of the mesh to invert the anomaly data. While the horizontal geometry of the mesh can be decided upon by analyzing the horizontal shape of the anomaly, the vertical extension is more problematic and an optimal choice of it allows a reduction of the number of layers, increasing the numerical performance of the inversion itself.

[21] If an optimal value of the DTB parameter exists, it should manifest itself in the data, for example by minimizing or maximizing some function. This approach resembles the L curve method for evaluating the optimal λ of equation (2). In that case a set of preliminary inversions at various λ was performed, and the optimal value was obtained by maximizing the curvature of the resulting plot of $\log |\mathbf{L} \cdot \mathbf{p}|^2$ versus $\log |\mathbf{K} \cdot \mathbf{p} - \mathbf{d}|^2$. In the case of equation (11), we seek a particular function showing a well-defined stationary point for the optimal value of z_0 . The functionals commonly used as additional bounds in the inversion methods (i.e., the chi-square norm, different L^n norms of the solution, the optimal λ parameter, the volume and the moment of inertia of the source) typically show monotonic behaviors with DTB. This can be easily understood for the chi-square norm or for the volume and moment of inertia of the source, because putting magnetized cells at the upper layers of the mesh allows us to obtain very good solution in terms of data fitting with a small number of magnetized cells, which practically means models with small volume or moment of inertia. The same reasons explain the behavior of the various L^n norms, because the upper layers of the mesh can be magnetized with low susceptibility values causing small norms of the solutions [Oldenburg and Li, 2003;

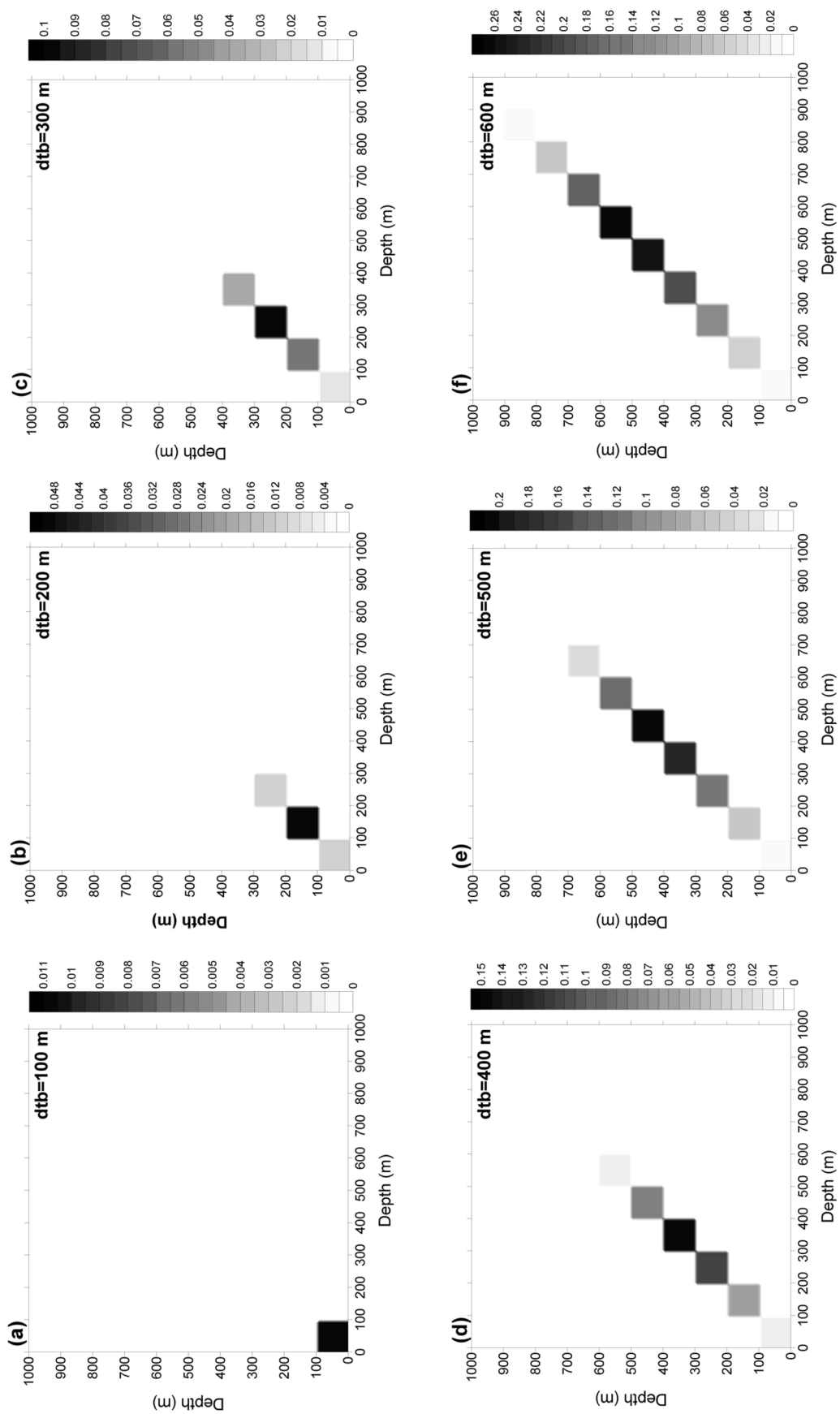


Figure 6. Plots of different regularization matrices for values of DTB from 100 to 600 m for the mesh of the model of Figure 3. Each block of the matrix represents a layer of the mesh since the data have been organized into a depth-descending order.

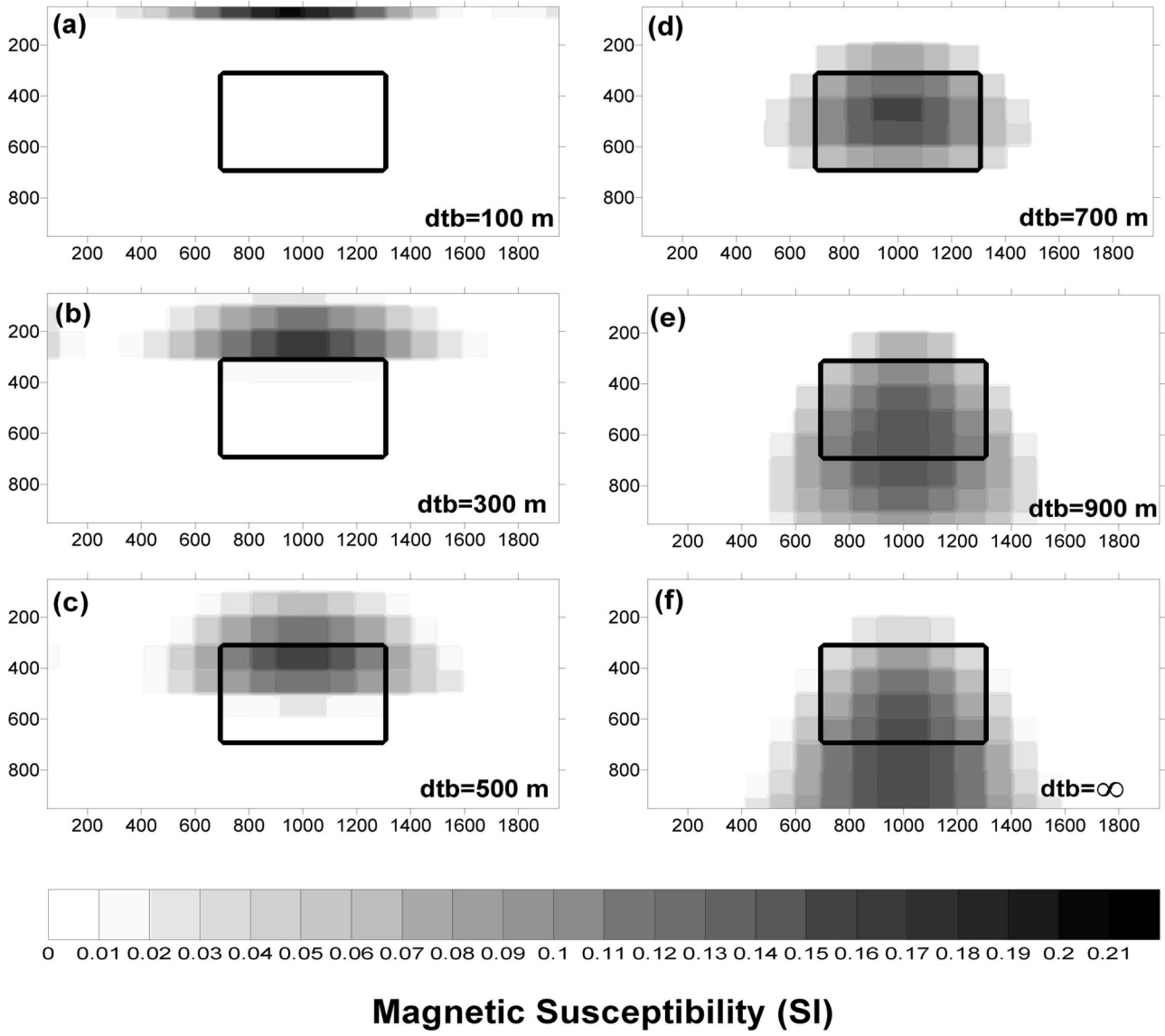


Figure 7. Results of inversions of the synthetic model of a prism buried at depth from 300 to 700 m. The magnetic susceptibility of the true source is 0.3 (SI). For each subplot the horizontal axis is north (m), while the vertical axis indicates the depth (m). The recovered models are evaluated by using different DTB parameters drawn in each subplot. In particular, Figure 7f indicates the result obtained by a power law regularization without the Fermi function effect, which corresponds to an infinite value of DTB. The recovered models show that the solution is shifted toward greater values of depth as the DTB parameter increases.

[Strykowski and Boschetti, 2003]. These functionals are thus useful during the inversion itself to obtain constrained models, but they cannot give information about the optimal DTB of equation (11).

[22] On the basis of numerical experiments, we found instead a norm of the model that gave meaningful results. The chosen regularization has a power law decay of 3/2 with depth for the first layers of the mesh, until the Fermi decay function is negligible. From this point of view the following N norm of the solution appears as a good candidate

$$N_{z_0} = \int_V \frac{|\chi_{z_0}(\mathbf{r})|}{z^{3/2}} dV, \quad (14)$$

where V is the volume of the mesh, \mathbf{r} indicates the position inside of this volume, and the magnetic susceptibility χ_{z_0} is obtained by the inversion at a determined z_0 . This quantity has been evaluated for different z_0 values and then plotted as a function of z_0 . The plot of this norm, having been tested by a large number of synthetic models, shows minimum values in proximity of a value of DTB that is close to the actual bottom depth of the source. Among the different solutions, each minimizing at the same time a misfit function and a regularizing functional characterized by a depth decay with a power law of 3/2, the optimal solution is characterized by the global minimum value of N norm. This norm is not completely empirical, since susceptibility and depth decay of the field are both present. The search for a

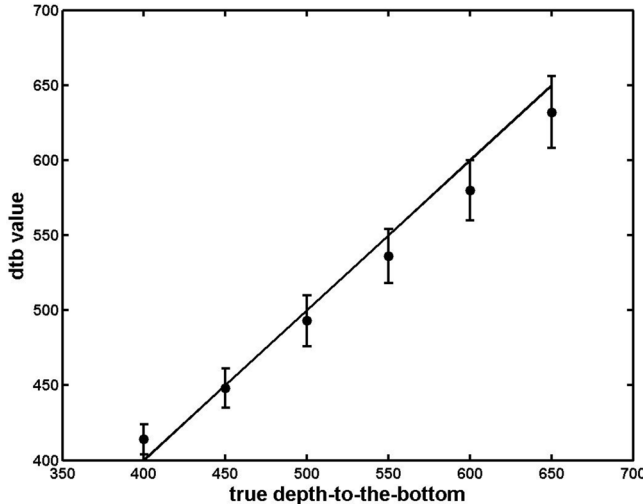


Figure 8. Plot of the minima of the N norm for the sources of Figure 9 with their error bars, compared with the true DTB represented by the linear trend.

minimum ratio between the numerator given by susceptibility and the denominator given by the depth decay prevents the source clustering at shallow depths, where $z^{-3/2}$ assumes large values, while the term $|\chi_{z_0}(\mathbf{r})|$ avoids also the existence of large susceptibility values, as happens when the best fitting solution is obtained at a depth larger than the true one.

[23] Before showing some synthetic tests to confirm these hypotheses, we summarize the main steps of the inversion method which proceeds as follows:

[24] 1. We define the mesh grid for the inversion with the straightforward prerequisite of enclosing the source. At this level the vertical extension of the mesh or the cell size of the grid is not so essential, since it can be optimized after having minimized the N norm. However, using a large mesh will ensure the proper closure of the source;

[25] 2. We run a set of fast preliminary inversions with a regularization matrix defined in equation (11) aimed at minimizing the N norm of the solution in terms of z_0 . The optimal DTB is found as the z_0 which minimizes the N norm;

[26] 3. The final inversion is performed with the obtained DTB that replaces z_0 in the regularization matrix of equation (11). The mesh grid at this level can be redefined, for example by neglecting layers deeper than DTB and increasing the number of layers shallower than DTB by reducing their thicknesses;

[27] 4. The recovered model is evaluated graphically in three dimensions, together with the statistical information pertaining to the chi-square optimization.

[28] Following this procedure we have inverted synthetic models of prisms with a thickness of 300 m, buried at different depths, with bottoms at every 50 m from 400 to 650 m. The inversions were performed by using the same mesh of the test of Figure 3. The preliminary analysis based on evaluation of minima of the N norm is shown in Figure 8, together with the true depth of the source that is represented

by the linear trend. The error associated to the DTB value is estimated in the following way:

[29] 1. We fit a polynomial function of order 6 to a discrete set of data of the N norm as a function of z_0 ;

[30] 2. We evaluate the error ΔN of the N norm as the average difference between the observed N norm and its interpolated value on the discrete points used to build the curve;

[31] 3. The minimization algorithm of the N norm proceeds by a Golden Section search and stops when some tolerance value of the N norm is assumed: as this tolerance value we choose the ΔN value calculated above;

[32] 4. The value of ΔN becomes a corresponding error Δd in the DTB value, by using the corresponding values on the N norm curve.

[33] Figure 9 shows the recovered models from the inversion performed by the DTB values shown as legend in each single plot. They are in good agreement. Once again, that the reduced chi-square norm χ^2/n was always close to 1, indicating a good and significant fit. The closing function also has the effect of reducing the L^2 norm of the solutions, so that in the final analysis for each separate case the L^2 norm was practically unchanged. The susceptibility values are slightly underestimated as the depth increases, since, obviously, the source is less accurately detected, but the distribution is peaked about the true center of the source and the structural trends of susceptibility are effectively determined. These results indicate that besides a correct DTB, our algorithm has given also a good approximation of the true susceptibility distribution.

[34] We now turn to studying the behavior of the N norm when moving from its optimal value, by analyzing Figure 7, where the true DTB parameter is 700 m. It is intuitively understandable that the regularization of equation (11) allows the inversion to activate vertical levels with depth shallower than z_0 , but drastically suppresses layers at depth greater than z_0 . The shallower solutions (Figures 7a and 7b) are characterized by a finite total susceptibility $\sum_i |\chi_i|$, whose value is not as much decreased as the increase of the average depth effect (Table 1). The large depth factor $z^{-3/2}$ plays the dominant role generating a large N norm. Increasing the value of $z_0 > 700$ m, as in Figures 7e and 7f, we note that cells placed inside of the true source maintain approximately the same susceptibility values, since the regularization permits to activate layers at a depth lower than z_0 . This effect, which is recognizable also in the numerical results of Table 1, is essential to preserve data fitting without altering the misfit function too much. Greater values of z_0 , however, allow the inversion to activate deeper layers, that do not contribute effectively to the predicted anomaly, but surely increase the N norm with a rate different than that which is given by the increase of the average depth effect as in Figures 7a and 7b. The optimal DTB is the minimum point at which this transition of behavior happens.

[35] This can be seen both by analyzing the numerical results of Table 1, and the example of Figure 10, which was obtained from another synthetic test, in which we study the asymmetric shape of the N norm around its minimum. We show in fact the application of this method to a more complex test, made of three separate sources at different depths. The inducing field is assumed to have an inclination

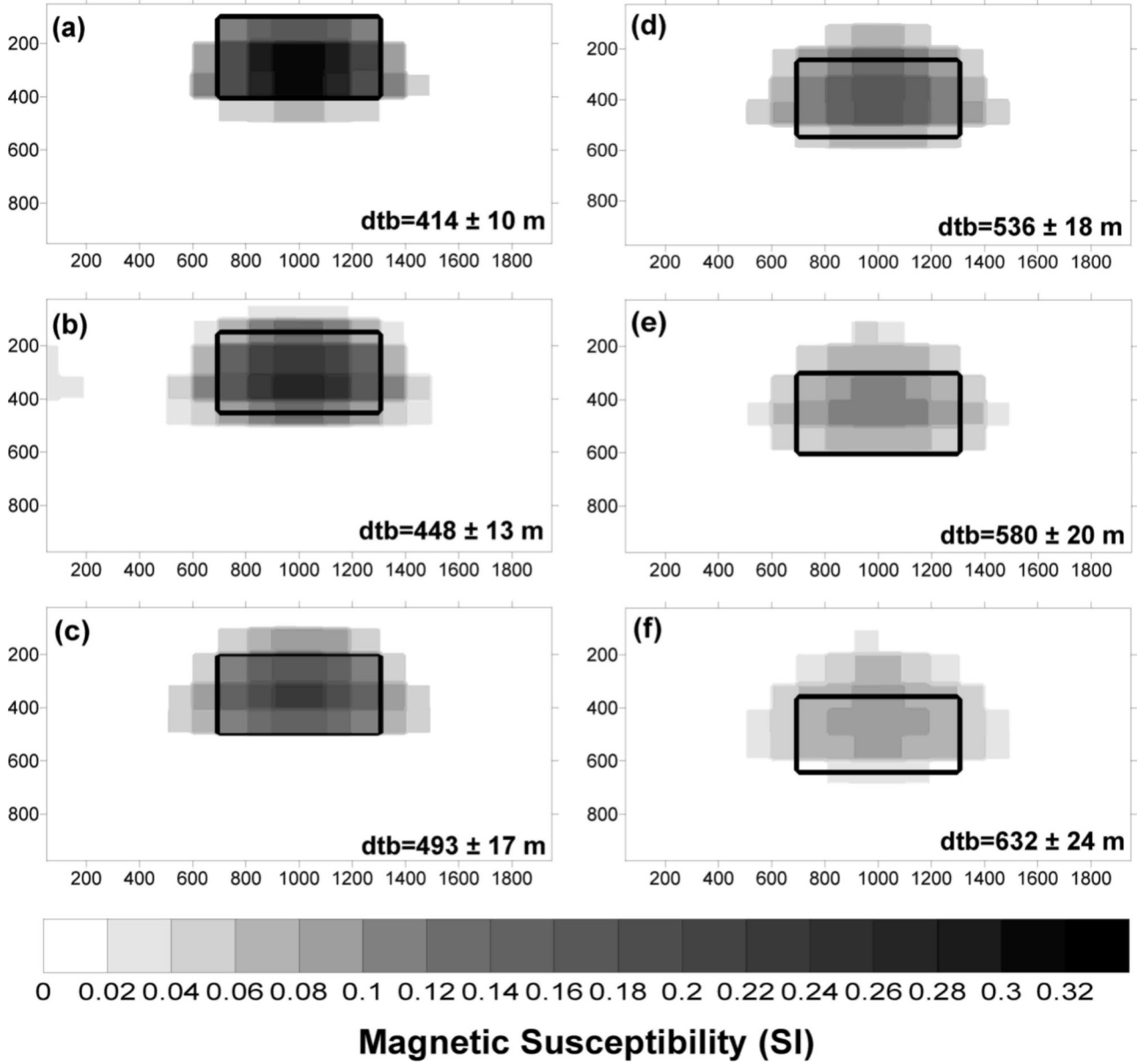


Figure 9. Results of inversions of synthetic models of prisms buried at different depths from 400 to 650 m every 50 m and relative DTB parameters. The magnetic susceptibility of the true source is 0.3 (SI). For each subplot the horizontal axis is north (m), while the vertical axis indicates the depth (m). The recovered models are in good agreement with the true sources, and the values of DTB reflect the actual values of the bottom depths of each prism. These values were obtained by minimization of the N norm.

of 45° , a declination of 45° and a magnitude of 40,000 nT. The magnetic anomaly map can be seen in Figure 11 where the distinct anomalies of each of the separate sources that compose the model are overlapped. We used a mesh made of $20 \times 20 \times 10$ voxels to invert the grid made of 20×20 data, to which we added Gaussian noise with a standard deviation of 3% of the data amplitude. In Figure 10 we show the plot of the N norm that gives a value of the $DTB = 770 \pm 35$ m. This value is in good agreement with the true value which is at 800 m. We have performed the inversion of the anomaly of Figure 11 by using the recovered $DTB = 770$ m, and $DTB = \infty$ that corresponds to using only a

power law regularization matrix. The corresponding L curves are shown in Figure 12, where Figure 12a indicates the solution at the correct DTB, while Figure 12b indicates the solution without DTB. The reduced chi-square norm for the model in Figure 12a is 0.55, while for the model in Figure 12b it is 0.49. The significance level of Figure 12a is thus 96% and 97% for Figure 12b, indicating a good fit in both cases. The L^2 norm of Figure 12b, approximately 1050, is instead considerably larger than the L^2 norm of Figure 12a at about 370, indicating that the deeper layers of the solution Figure 12b do not contribute effectively to fit the inverted anomaly, and generate a solution with a large

Table 1. Summary of the Numerical Results of Figure 7^a

Average Depth, m	Total Susceptibility	Depth Effect	<i>N</i> Norm	DTB
50	10.31	280×10^{-5}	29×10^{-3}	100
212	33.24	35×10^{-5}	12×10^{-3}	300
321	50.71	19×10^{-5}	9.7×10^{-3}	500
473	56.12	9.7×10^{-5}	5.4×10^{-3}	700
633	90.17	6.3×10^{-5}	5.6×10^{-3}	900
643	94.13	6.1×10^{-5}	5.8×10^{-3}	∞

^aThe average depth is computed by the cells with susceptibility greater than a tolerance value of 10^{-3} . The depth effect given by $z^{-3/2}$ is calculated as if the whole source was concentrated at the average depth. The *N* norm value is thus obtained by multiplying the depth effect with the total susceptibility.

L^2 norm. Figure 13 shows the comparison between the true source (Figure 13a) and the recovered models by means of horizontal cross sections. Introducing the DTB information by the Fermi function produces a more realistic result, with a correct closure of the source toward its bottom as can be seen in Figure 13b, while the susceptibility magnitude and its distribution resemble the true source. In contrast Figure 13c shows the inverse model coming from a simple power law regularization matrix. We can see that this solution is still extended toward the bottom of the mesh, reflecting, however, the difference in depth among the separate sources that compose the global model.

[36] Before showing the performance of the inversion method applied to a set of real magnetic anomalies, we discuss the main results shown by the synthetic tests. It is obvious that the assumptions made for the synthetic tests are not always valid in the real case, so that our algorithm may have some restrictions when applied to more general situations. We discuss briefly such possible limitations and difficulties. We recognize that the choice of the Fermi function is the critical element, especially since it is used

to obtain the optimal DTB by the *N* norm minimization. Other functions may be adopted and this can be a point open to further research. One of the weaknesses of the Fermi function is that it drastically suppresses layers deeper than DTB, practically assuming a single source along the vertical profile. On the one hand this is essential to provide the optimal DTB, but on the other it can show some difficulties in the case of vertically overlapping sources or extremely dipping bodies, where the Fermi function alone will give a single source vertically extending about the center of magnetization of the real source. The detection of a magnetic basement or the Curie isotherm can be problematic unless the crustal portion that is magnetically detectable actually matches the bottom of the shallower magnetic sources. This may happen in volcanic regions characterized by a thick crust. Last, the induced magnetization hypothesis, unless it is supported by rock samples data or other information, may not be met in real applications, and its validity can be questioned by analyzing the recovered model to see if large zones with intense negative susceptibility are found, as happens in the case of extremely dipping bodies. It is likely that some of these potential shortcomings may be alleviated by introducing further constraints that may be easily added to the proposed method, such as focusing techniques [Portniaguine and Zhdanov, 2002]. Nevertheless, judging from the good results obtained in DTB determination, we propose our algorithm as an easy alternative: it gives first-order solutions with good depth resolution, both for the top and the bottom of the source, which is particularly useful for surveys where the user knows a minimal amount of “*a priori*” information about the real source.

5. Volcanic Centers of the Latium Region

[37] We applied the inversion algorithm to the geologic-volcanic pattern connected to the outcropping Miocene-

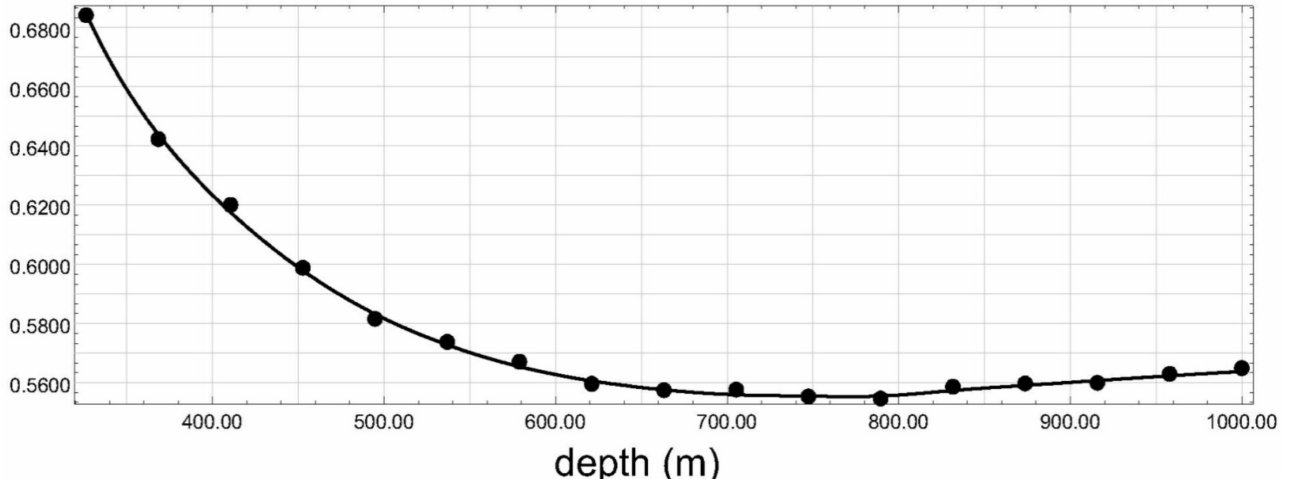


Figure 10. Plot of the minimization curve of the *N* norm for evaluating the DTB parameter from the synthetic anomaly data of Figure 11. The dots indicate the points where the *N* norm has been evaluated, while the solid line is a polynomial interpolation of order 6. The optimal value of DTB is 770 ± 35 m, which is in good agreement with the true value of 800 m as can be seen in the model of Figure 12. The asymmetric behavior of the *N* norm around its minimum is well visible.

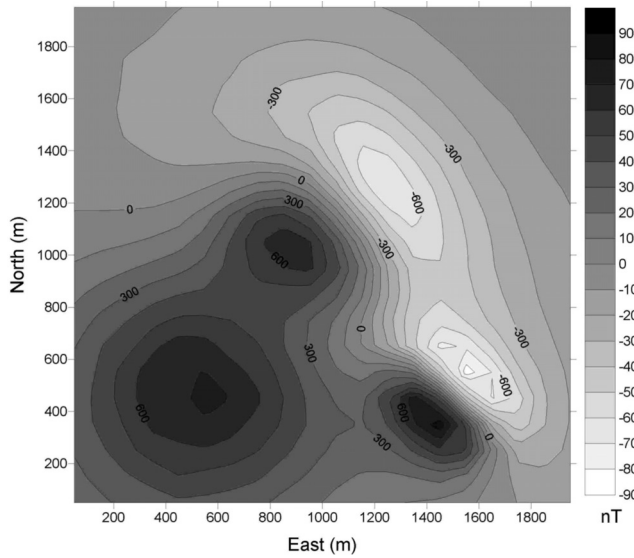


Figure 11. Synthetic anomaly generated by a composite prismatic model. The inducing field is assumed to have an inclination of 45° , a declination of 45° , and a magnitude of 40,000 nT. The anomaly is calculated by a grid of 20×20 points. Random Gaussian noise with a standard deviation of 3% of the data magnitude has been added to the data.

Quaternary magmatism of the Latium Region in Italy. The volcanoes of the Northern Latium Center are located on the Tyrrhenian margin of Italy westward of the compressional front of the Apennine-Maghrebian chain. The magmatic pattern shows a NW-SE trend and covers four singular volcanics complexes (toward SE): Vulsini, Vico, Sabatini and Albani. The volcanism of the Latium area begun in the Pleistocene (about 0.6–0.4 Ma) [Serri et al., 2001] and reached its end around 0.1 Ma. The Albani system had more recent activity since 0.02 Ma [Marra et al., 2004]. These volcanic structures are the northwestern evidence of the potassic-ultrapotassic Roman Magmatic Province [Washington, 1906]. The potassic-ultrapotassic magmatism of the Latium region is strongly connected with the Tertiary compressional system and is related to intense block faulting and rifting developed between Upper Miocene and Present in the western side of the Apennine chain [Beccaluva et al., 1991]. The geochemical features of the Latium area are related to the undersaturated chemistry of the other magmatic centers of the central Italy (Campanian Region–Vulture). They are connected with distinct enrichment of the mantle sources [Serri, 1990; Serri et al., 2001]. Figure 14 shows the magnetic anomaly pattern of the Latium region, located near Rome. This map derives from the digital database of the aeromagnetic anomaly field of Italy of the Oil Company Eni Exploration and Production Division. The anomaly field, after the standard leveling, has been obtained by DGRF (Definitive Geomagnetic Reference Model) sub-

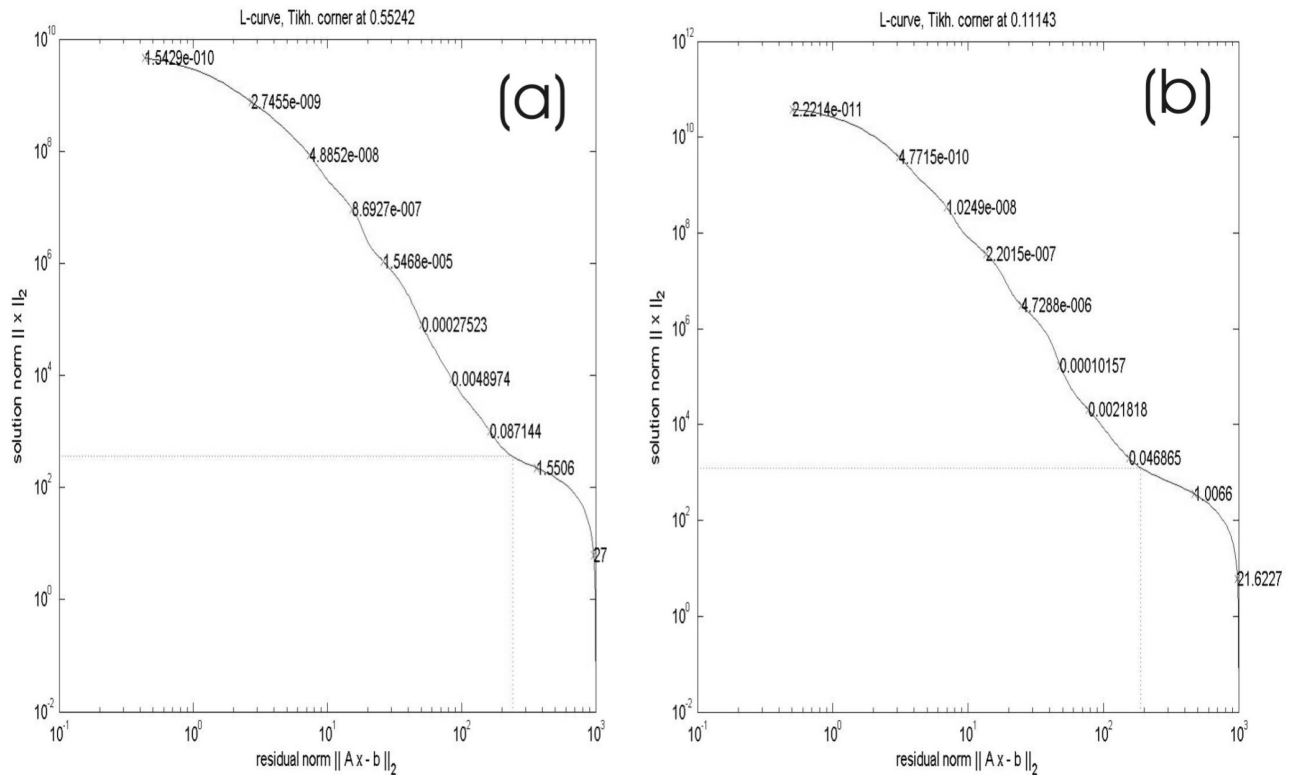


Figure 12. L curves coming from the inversion of the anomaly of Figure 11 (a) in the case of $DTB = 770$ m and (b) with $DTB = \infty$. The chi-square norm of the model in Figure 12a is slightly larger than that of Figure 12b, but the L^2 norm is considerably larger in the case of Figure 12b, showing that the deep layers do not contribute effectively to fit the observed anomaly.

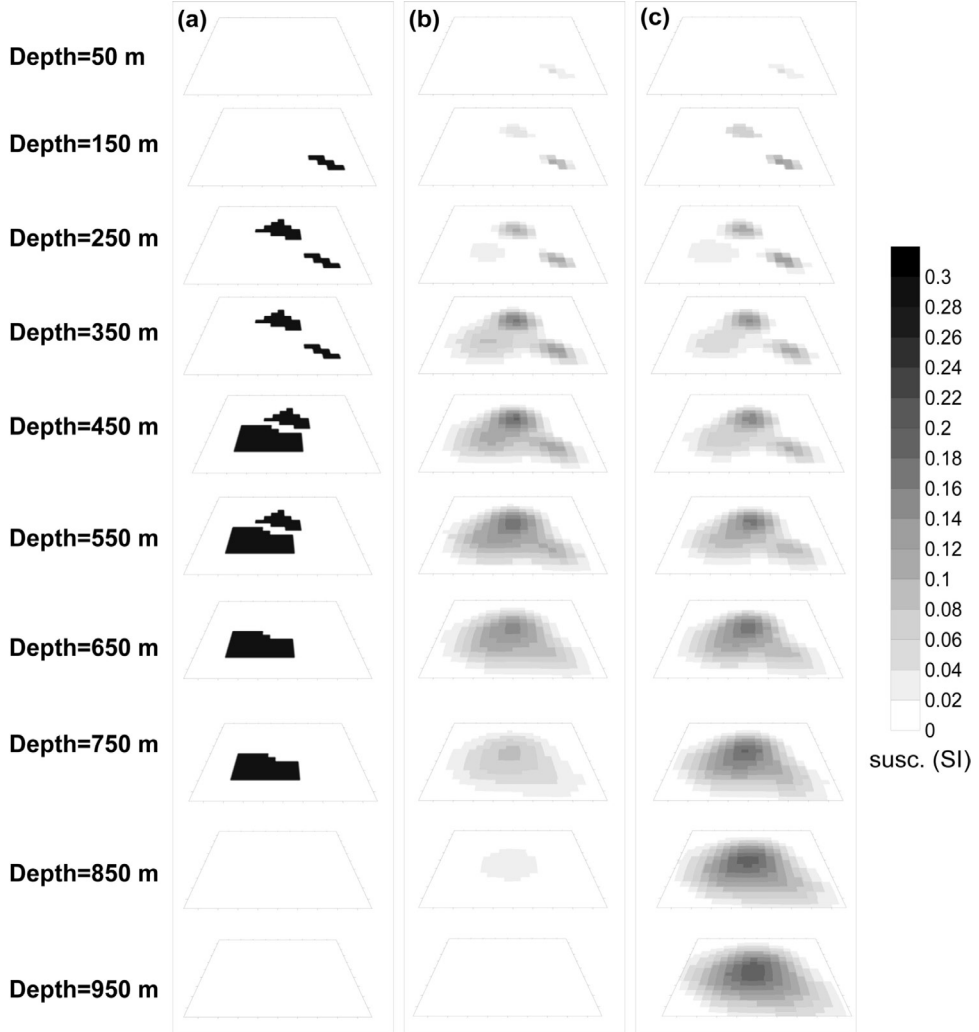


Figure 13. Recovered model from inversion of synthetic anomaly data of Figure 11 represented by horizontal cross sections at various depths. The data were inverted by using a mesh of $20 \times 20 \times 10$ voxels, centered about the anomaly of Figure 11, thus extending from 0 to 2000 m for each horizontal direction and from 0 to 1000 m for the vertical axis. (a) True susceptibility model, (b) recovered model with $DTB = 770$ m, and (c) recovered model with $DTB = \infty$ that corresponds to using only a power law decay regularization matrix. Figures 13b and 13c are similar for the first cross sections, but while the model in Figure 13b is closed toward its bottom at the correct depth, the solution in Figure 13c appears still pushed toward the bottom of the mesh.

traction for the geomagnetic epoch 1979.0. The data were recorded at an observation level of 1460 m, the projection is a transverse Mercator with reference latitude at 0° , reference longitude at 14° , false east at 1,500,000 m and false north at 0 m [Caratori Tontini et al., 2004].

[38] The boxes in Figure 14 indicate three distinct anomalies that have been separately inverted by our algorithm. These anomalies are interpreted to be magnetic signatures of the magmatism of the region. The Vulsini complex is represented by anomaly A, the Vico-Sabatini anomaly is enclosed by the box B, while C is the anomaly of the Albani complex. The very similarity of these anomalies as regards their amplitude and typical wavelengths allows the extraction of these anomalies from the relatively flat background, and

suggests a common nature. The induced magnetization hypothesis is justified because of the young age of this volcanic complex, whose origin is more recent than the last polarity inversion, so that if remanent magnetization is present it is aligned with the ambient-inducing field [Marra et al., 2004]. Each separate anomaly, gridded with a cell size of 1.5 km, has been inverted by our algorithm by using a mesh centered under the anomaly made of $30 \times 30 \times 15$ voxels. The vertical extension of the mesh sizes from 500 m above sea level to 13,500 m below sea level. The DTB analysis yielded a common value of 12.0 ± 0.6 km for anomalies A and C, while anomaly B showed a $DTB = 10.1 \pm 0.5$ km. Figure 15 shows the results of the inversions by horizontal cross sections that allow comparison between the sources.

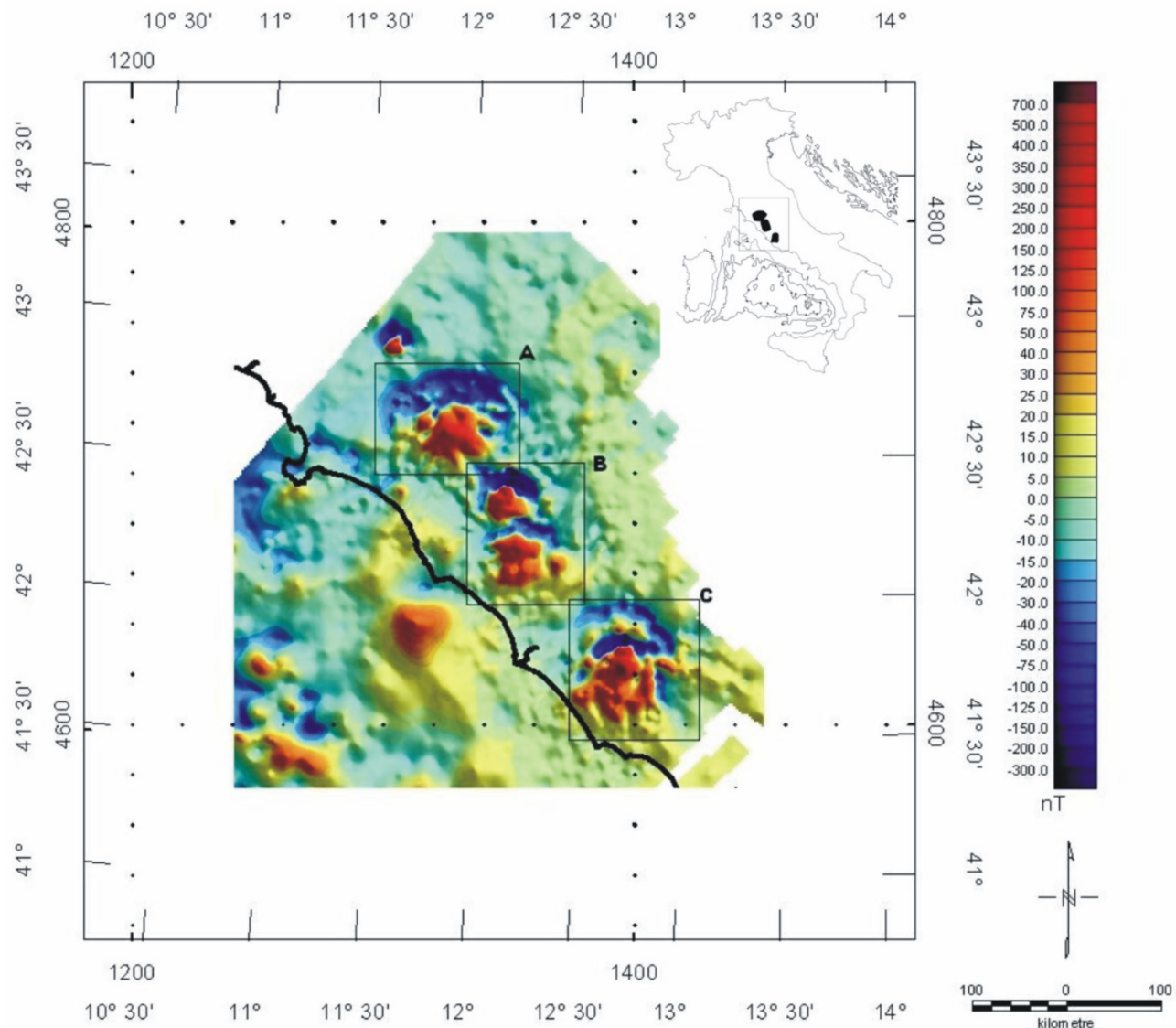


Figure 14. Magnetic pattern of the investigated volcanic structures of the Latium region at an observation level of 1460 m. Three magnetic anomalies, indicated by the boxes A, B, and C, were isolated and inverted. The solid black line represents the Italian coastline, and westward is the Tyrrhenian Sea. The map is a transverse Mercator projection with reference latitude at 0°, reference longitude at 14°, false east at 1,500,000 m, and false north at 0 m.

The geometry and extension of the sources in the deep layers is typical for this kind of magmatic chambers that are characterized by a circular shape. Typical rise-up structures are evident in the shallow sections, converging at depth into four isolated magmatic chambers. It is interesting to compare the outcropping evidence of these volcanic structures with our recovered model. To this aim we have projected the first horizontal cross section over the topographic shaded relief (Figure 16). This section ranges from 500 m above sea level to 500 m below sea level and is compatible with the maximum topographic relief of 460 m. The susceptibility is located over topographic highs connected with the outcropping volcanic edifices. The

recovered susceptibility values are in the range $0\text{--}10^{-3}$ black which is dimensionless in SI units. These values are in good agreement with rock samples from this area [Porreca *et al.*, 2003]. Some ring-shaped susceptibility patterns moreover identify the border of the rims that in this region are evident in the form of volcanic lakes. These calderic structures are well visible in Figure 16. This is an important characteristic of this volcanic region, since the calderization process tends sometimes to change the magnetic features of rocks because of the collapse of the main conduit that alters the susceptibility pattern. This is mainly due to a mixing with terrigenous sediments with very low susceptibility values. The separate structures recovered by our model

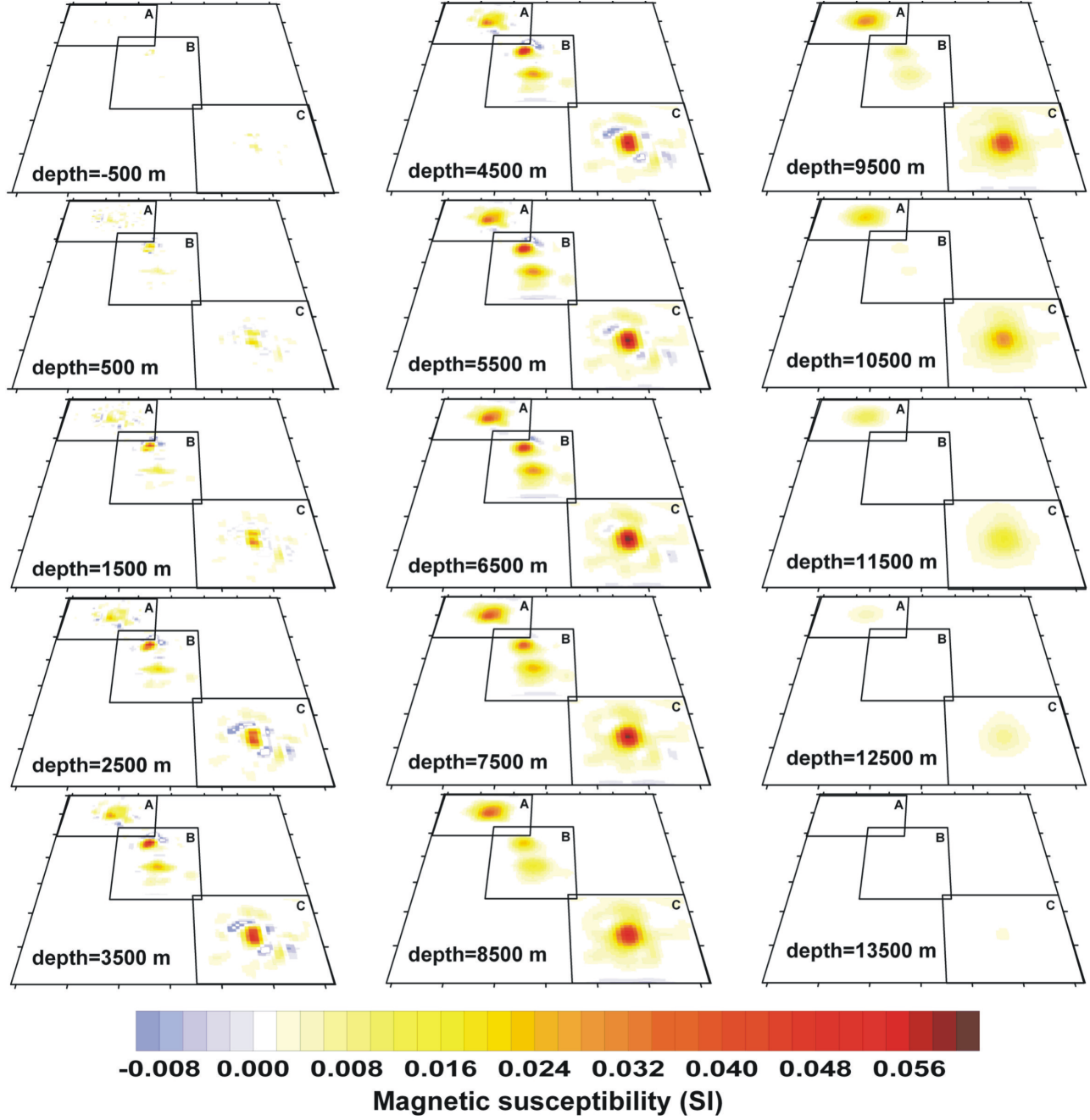


Figure 15. Recovered model from inversion of the system of anomalies of the Roman Magmatic Province shown in Figure 13. Each inversion has been performed by using a mesh of $30 \times 30 \times 15$ voxels centered under the anomaly. The global horizontal extension of each cross section is east = [1300,1420] km and north = [4600,4740] km. The coordinate system is the same as Figure 12.

show similar susceptibility values and geometries, suggesting that probably they have a deep common mantle origin that during rise up has been differentiated according to the model of Figure 15.

6. Conclusions

[39] We have developed an inversion algorithm for magnetic data by inserting a depth-weighting function into the model regularization function, modified from *Li and*

Oldenburg [1996]. We have transformed this problem into a simple “free” inversion with minimization of an L^2 norm, increasing the numerical performance of the algorithm that thus is particularly effective for fast applications. The depth-weighting function depends on one parameter that is connected with the depth to the bottom of the source and allows the closure of the source toward its bottom at a consistent depth. We have shown how this DTB parameter can be found from the data by a first inversion step. Synthetic tests have been performed to ascertain the reli-

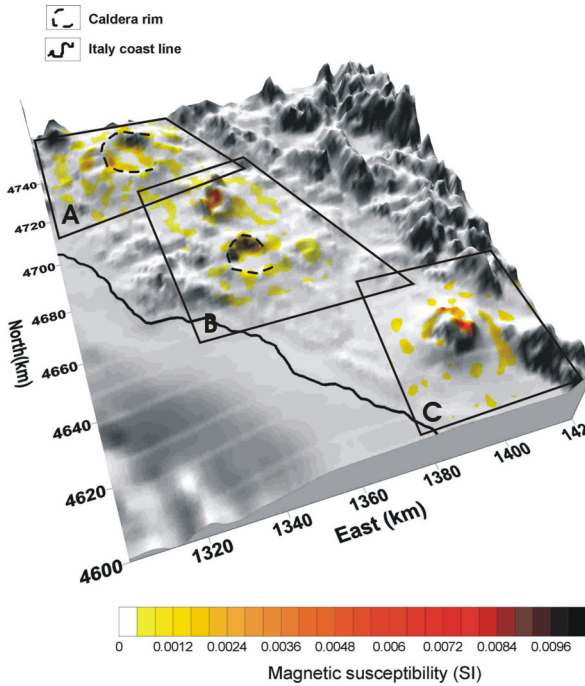


Figure 16. First cross section of the recovered model of Figure 14 projected over the shaded topographic relief of the region investigated by the inversion algorithm. The first section of Figure 14 describes actually outcropping structures since it is evaluated from 500 m above sea level to 500 m below sea level.

ability of the method and a set of three anomalies of volcanic origin in Italy have been inverted, obtaining a model that is in good agreement with the available geological information and the topographic evidence of the region.

[40] While we have shown examples of magnetic anomalies, a similar algorithm has been successfully tested on gravity data, provided an appropriate change of parameters. We have shown examples of optimization curves to evaluate the depth-to-the-bottom parameter, but this procedure is embedded in the algorithm itself by a fast preliminary analysis. Some limitations have also been discussed in order to highlight possible future improvements. The method allows the user to obtain realistic models and can be also used to have a quantitative evaluation of the DTB of the source even for large-scale anomalies, for example in Curie depth or magnetic basement evaluation. When possible and if it is allowed by the crustal regime of the investigated region, we can extract a set of windowed subanomalies and separately analyze them to find a DTB for each anomaly. The global superposition of the DTBs can thus provide a map of the magnetic basement. In conclusion, this is a promising method, which we are working on extending to more complex source geometries.

[41] **Acknowledgments.** We thank Eni Exploration and Production Division and particularly I. Giori for the use of the magnetic data. We are indebted to AE F.J. Simons for his significant help in improving the level of this work, and we thank Erwan Thébault and an unknown reviewer for their useful comments. P. C. Hansen is particularly appreciated for having made available the Matlab routines for regularization tools that have been used in

the algorithm (www.imm.dtu.dk/~pch). Finally, we thank Lynden Cronin for having corrected the English style. F.C.T. wishes to dedicate this paper to his little Riccardo.

References

- Andersen, F. H., and L. B. Pedersen (1979), Some relations between potential fields and the strength and center of their sources, *Geophys. Prospect.*, **27**, 761–774.
- Barbosa, V. C. F., and J. B. C. Silva (1994), Generalized compact gravity inversion, *Geophysics*, **59**, 57–68.
- Beccaluva, L., P. Di Girolamo, and G. Serri (1991), Petrogenesis and tectonic setting of the Roman Volcanic Province, *Lithos*, **26**, 191–221.
- Bhattacharyya, B. K. (1964), Magnetic anomalies due to prism-shaped bodies with arbitrary polarization, *Geophysics*, **29**, 517–531.
- Bhattacharyya, B. K., and L. K. Leu (1975), Analysis of magnetic anomalies over Yellowstone National Park: Mapping Curie point isothermal surface for geothermal reconnaissance, *J. Geophys. Res.*, **80**, 4461–4465.
- Blakely, R. J. (1988), Curie temperature isotherm analysis and tectonic implications of aeromagnetic data from Nevada, *J. Geophys. Res.*, **93**, 11,817–11,832.
- Blakely, R. J. (1995), *Potential Theory in Gravity and Magnetic Applications*, Cambridge Univ. Press, New York.
- Boulanger, O., and M. Chouteau (2001), Constraints in 3D gravity inversion, *Geophys. Prospect.*, **49**, 265–280.
- Caratori Tontini, F., O. Faggioni, N. Beverini, and C. Carmisciano (2003), Gaussian envelope for 3D geomagnetic data inversion, *Geophysics*, **68**, 996–1007.
- Caratori Tontini, F., P. Stefanelli, I. Giori, O. Faggioni, and C. Carmisciano (2004), The revised aeromagnetic anomaly map of Italy, *Ann. Geophys.*, **47**, 1547–1555.
- Claerbout, J. F. (1976), *Fundamentals of Geophysical Data Processing With Applications to Petroleum Prospecting*, McGraw-Hill, New York.
- Connard, G., R. Couch, and M. Gemperle (1983), Analysis of aeromagnetic measurements form the Cascade Range in central Oregon, *Geophysics*, **48**, 376–390.
- Fedi, M., and A. Rapolla (1999), 3-D inversion of gravity and magnetic data with depth resolution, *Geophysics*, **64**, 452–460.
- Guillen, A., and V. Menichetti (1984), Gravity and magnetic inversion with minimization of a specific functional, *Geophysics*, **49**, 1354–1360.
- Hansen, P. C. (1994), Regularization tools: A Matlab package for analysis and solution of discrete ill-posed problems, *Numer. Algorithms*, **6**, 1–35.
- Hansen, P. C., and D. P. O’Leary (1993), The use of the L-curve in the regularization of discrete ill-posed problems, *SIAM J. Sci. Comput.*, **14**, 1487–1503.
- Helbig, K. (1963), Some integrals of magnetic anomalies and their relation to the parameters of the disturbing body, *Z. Geophys.*, **29**, 81–96.
- Ho-Liu, P., J.-P. Montagner, and H. Kanamori (1989), Comparison of iterative back-projection inversion and generalized inversion without blocks: Case studies in attenuation tomography, *Geophys. J. Int.*, **97**, 19–29.
- Jacobsen, B. H. (1987), A case for upward continuation as a standard separation filter for potential field maps, *Geophysics*, **52**, 1138–1148.
- Landau, L. D., and E. M. Lifshits (1977), *Statistical Physics*, MIR, Moscow.
- Last, B. J., and K. Kubik (1983), Compact gravity inversion, *Geophysics*, **48**, 713–721.
- Lawson, C. L., and R. J. Hanson (1974), *Solving Least Squares Problems*, Prentice-Hall, Upper Saddle River, N. J.
- Li, Y., and D. W. Oldenburg (1996), 3-D inversion of magnetic data, *Geophysics*, **61**, 394–408.
- Marra, F., J. Taddeucci, C. Freda, W. Marzocchi, and P. Scarlato (2004), Recurrence of volcanic activity along the Roman Comagmatic Province (Tyrrenian margin of Italy) and its tectonic significance, *Tectonics*, **23**, TC4013, doi:10.1029/2003TC001600.
- Maus, S., D. Gordon, and D. Fairhead (1997), Curie-temperature depth estimation using a self-similar magnetization model, *Geophys. J. Int.*, **129**, 163–168.
- Menke, W. (1989), *Geophysical Data Analysis: Discrete Inverse Theory*, Elsevier, New York.
- Okubo, Y., and T. Matsunaga (1994), Curie point depth in northeast Japan and its correlation with regional thermal structure and seismicity, *J. Geophys. Res.*, **99**, 22,363–22,371.
- Oldenburg, D. W., and Y. Li (2003), Discussion on “3-D inversion of gravity and magnetic data with depth resolution”, *Geophysics*, **68**, 400–403.
- Pedersen, L. B. (1991), Relations between potential fields and some equivalent sources, *Geophysics*, **56**, 961–971.
- Pignatelli, A., I. Niccolosi, and M. Chiappini (2006), An alternative 3D source inversion method for magnetic anomalies with depth resolution, *Ann. Geophys.*, in press.
- Pilkington, M. (1997), 3-D magnetic imaging using conjugate gradients, *Geophysics*, **62**, 1132–1142.

- Porreca, M., M. Mattei, G. Giordano, D. De Rita, and R. Funiciello (2003), Magnetic fabric and implications for pyroclastic flow and lahar emplacement, Albano maar, Italy, *J. Geophys. Res.*, 108(B5), 2264, doi:10.1029/2002JB002102.
- Portniaguine, O., and M. S. Zhdanov (2002), 3-D magnetic inversion with data compression and image focusing, *Geophysics*, 67, 1532–1541.
- Scales, J. A., and R. Snieder (1997), To Bayes or not to Bayes?, *Geophysics*, 62, 1045–1046.
- Serri, G. (1990), Neogene-Quaternary magmatism of the Tyrrenian region: Characterization of the magma sources and geodynamic implications, *Mem. Soc. Geol. It.*, 41, 219–242.
- Serri, G., F. Innocenti, and P. Manetti (2001), Magmatism from Mesozoic to Present: Petrogenesis, time-space distribution and geodynamic implications, in *Anatomy of an Orogen: The Apennines and Adjacent Mediterranean Basins*, edited by G. B. Vai, and I. P. Martini, pp. 77–103, Springer, New York.
- Shuey, R. T., D. K. Schellinger, A. C. Tripp, and L. B. Alley (1977), Curie depth determination from aeromagnetic spectra, *Geophys. J.R. Astron. Soc.*, 50, 75–101.
- Silva, J. B. C., W. E. Medeiros, and V. C. F. Barbosa (2001), Potential-field inversion: Choosing the appropriate technique to solve a geological problem, *Geophysics*, 66, 511–520.
- Simons, F. J., R. D. van der Hilst, J.-P. Montagner, and A. Zielhuis (2002), Multimode Rayleigh wave inversion for heterogeneity and azimuthal anisotropy of the Australian upper mantle, *Geophys. J. Int.*, 151, 738–754.
- Strykowski, G., and F. Boschetti (2003), Discussion on “3-D inversion of gravity and magnetic data with depth resolution”, *Geophysics*, 68, 403–405.
- Tarantola, A. (1987), *Inverse Problem Theory*, Elsevier, New York.
- Tarantola, A., and B. Valette (1982), Generalized nonlinear inverse problems solved using the least squares criterion, *Rev. Geophys.*, 20, 219–232.
- Tikhonov, A. N., and V. Y. Arsenin (1977), *Solutions of Ill-Posed Problems*, Winston, Washington, D. C.
- Washington, H. S. (1906), *The Roman Comagmatic Region*, 199 pp., Carnegie Inst., Washington, D. C.
- Yanovskaya, T. B., and P. G. Ditmar (1990), Smoothness criteria in surface wave tomography, *Geophys. J. Int.*, 102, 63–72.
- Zhdanov, M. S. (2002), *Geophysical Inverse Theory and Regularization Problems*, Elsevier, New York.

F. Caratori Tontini and C. Carmisciano, Stazione di Geofisica Marina, Istituto Nazionale di Geofisica e Vulcanologia, via Pezzino Basso 2, I-19020 Fezzano (SP), Italy. (caratori@ingv.it; carmisciano@ingv.it)

L. Cocchi, Dipartimento Scienze della Terra Geologiche-Ambientali, Università di Bologna, P.zza Porta S. Donato 1, I-40126 Bologna, Italy. (cocchi@ingv.it)